Microstructures and Structural Properties of Sol−Gel Silica Foams

Elise Berrier,[†] Carine Zoller,[‡] Franck Beclin,[‡] Sylvia Turrell,[§] Mohamed Bouazaoui,*[,†] and Bruno Capoen[†]

Laboratoire PhLAM (CNRS, UMR 8523), Laboratoire LSPES (UMR8008) and Laboratoire LASIR (8516), Centre d'Etudes et de Recherches Lasers et Applications (CERLA), and Université des Sciences et Technologies de Lille, Villeneuve d'Ascq F-59655, France

Received: June 9, 2005; In Final Form: October 3, 2005

Silica xerogels were synthesized and annealed at 1000 °C for different durations to yield stable silica materials. The samples were prepared through base-catalyzed hydrolysis and condensation of tetramethyl orthosilicate in methanol. After aging and drying steps, clear and solid xerogels exhibiting a narrow pore size distribution were achieved. The annealing treatment of these xerogels was performed at 1000 °C and proved in the present study to lead to a monolithic glass when a progressive heat-treatment procedure was employed to attain 1000 °C. In addition to the expected glass, silica foams and ordered phases were observed when the samples were instantaneously heat-treated at 1000 °C. Raman spectra of the foamed materials exhibit the classical features of amorphous silica, whereas transmission electronic microscopy pictures reveal the presence of crystallized domains within the vitreous matrix. These crystallites are prone to nucleation and growth processes, which jeopardize the believed stability of the silica foam. The assessment of the hydroxyl content by IR spectroscopy reveals the role played by the latter polycondensation of silanols. The occurrence of foaming process was thus found to result from two competitive phenomena occurring at 1000 °C: evacuation of water-related species and viscous sintering.

I. Introduction

Sol−gel products distinguish themselves from other new materials by yielding promising monoliths that can be suitable for a large field of applications, including glasses for optical components[1] and the production of biocompatible materials.[2] The densification process of silica xerogels is accompanied by an important modification of the silica network and of specific structural entities, such as three- and four-membered silica rings. The gel-to-glass transition involves viscous sintering and shrinkage phenomena[3] and requires moderate temperatures. Indeed, the range of 900−1200 °C is commonly used to convert gel materials into glass compounds. The sol−gel-derived glass appears to be identical to that yielded by the classical melt−quench process.[4] The macroscopic properties such as structure, density, refractive index, as well as absorption are comparable. More precisely, X-ray diffraction and Raman spectra of the two glasses are quite similar. However, these systems differ from each other in their behavior at high temperatures. Indeed, one can discuss the stability of the sol−gel-derived glass in comparison with the melt one. Matsuyama et al.[5] have investigated this point and reported the study of the foaming of sol−gel materials during consolidation at 1000 °C and at higher temperatures around 2000 °C. A distinction was made between two types of foaming. Foaming I occurs at moderate temperatures (900−1100 °C) and generates a cloudy central core within the xerogel showing no particular structure by X-ray diffraction, whereas type II is associated with higher temperatures (2000 °C and above). The first type of foam appears to be related mainly to the initial density of the xerogel. A recent work reported by Kurumada et al.[6] tends to support this statement using acid and base media for sol preparation.

The purpose of the present work is the combined use of vibrational spectroscopies (Raman, IR) and electronic microscopy (scanning electron microscopy (SEM) and transmission electron microscopy (TEM)) to investigate both the structural and microstructural characteristics of silica foams and glasses.

The starting xerogel samples were prepared through hydrolysis and condensation of a silica-based alkoxide, followed by conventional aging and stabilization steps. Further heat treatment was pursued but with no step for the OH-removal step (i.e., chlorine treatment), thus allowing OH-containing species to be trapped inside the gel. The aging and stabilization treatments have been tuned to be soft and progressive enough to avoid cracks inside the material. During the densification treatment, two phenomena occurred depending on the annealing conditions: either a "type I foamed silica" or a stable glass were found to occur at 1000 °C. After a determined heat-treatment procedure, we proved that the phenomenon of polycondensation still occurs inside the monolith at 1000 °C, leading to the formation of water molecules trapped inside the structure. In this case, most of the porosity collapses before complete removal of these residual water under pressure, allowing the achievement of new features at moderate temperatures: type I foaming and crystallites.

II. Experimental Section

II.1. Sample Preparation. Gel monoliths were synthesized by hydrolysis and condensation of tetramethyl orthosilicate (TMOS, Aldrich) under basic conditions (ammonia) in the presence of methanol (Aldrich). TMOS, water, and methanol

* To whom correspondence should be addressed. E-mail: mohammed.bouazaoui@univ-lille1.fr. Phone: (33) 3 20 43 68 26. Fax: (33) 3 20 33 64 63.
[†] Laboratoire PhLAM (UMR 8523), Université Lille 1.
[‡] Laboratoire LSPES (UMR 8008), Université Lille 1.
[§] Laboratoire LASIR (UMR 8516), Université Lille 1.

10.1021/jp053089+ CCC: $30.25
Published on Web 11/10/2005

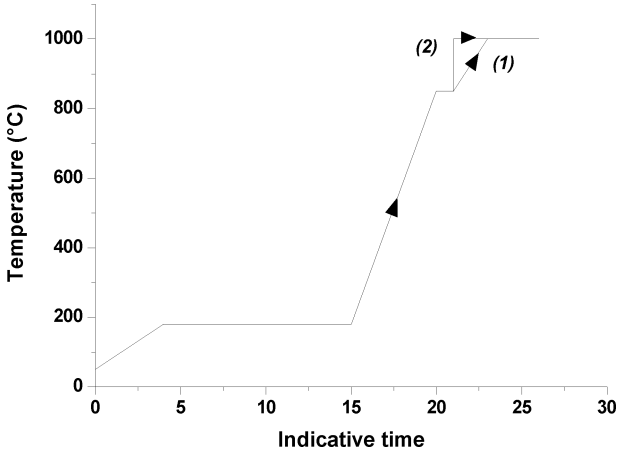

Figure 1. Schematic diagram of the heat-treatment procedures: procedure 1, "progressive" yielding a sol−gel-derived glass; procedure 2, "fast way" yielding a silica foam.

were mixed in the molar ration 1:10:4 and *N*-dimethylformamide (DMF) was added as drying control chemical additive (DCCA). The sol was vigorously stirred and poured into polypropylene flasks for gelation. Afterward, the gels were aged at 50 °C, and once the opaque stage was complete, they were slowly heated (0.1 °C/min) to 850 °C under atmospheric conditions. Stabilization of the xerogels was achieved by annealing the samples at 850 °C for 1 h. After this "stabilization treatment", the low-density monoliths were heat treated at 1000 °C under atmospheric conditions for various durations ranging from one to thirty hours.

Figure 1 shows typical temperature procedures for annealing of silica xerogels. As shown, the densification temperature of 1000 °C was reached either progressively (1) or by direct heating (2).

II.2. Characterization of Silica Samples.

II.2.1. Density Measurements. Apparent density values were determined through a simple mass-to-volume ratio. Sample weight was measured with an accuracy of $\pm 2 \times 10^{-4}$ g, and the dimensions were measured using a micrometer (precision $= \pm 0.01$ mm). The density measurements make it possible to quantify the degree of shrinkage or expansion of the materials.

II.2.2. Raman Spectroscopic Investigations. Raman spectra were recorded at room temperature using the 514.532-nm line of an argon ion laser as an excitation source with power levels ranging from 200 to 650 mW. Both macroscopic and microscopic configurations were used to study the structural evolution of the gels. The scattered light was collected using a Jobin-Yvon T64000 spectrometer coupled with a nitrogen-cooled charge-coupled device camera. The spectral range investigated in the present work was 10−1600 cm^{-1}, with a typical spectral slit width of 0.5 cm^{-1}.

II.2.3. Textural Analysis. Nitrogen adsorption−desorption (A−D) isotherms were recorded at 77.35 K using a Quantachrome porosimeter Autosorb 1-LP-MP after an outgassing of several hours at 150 °C under secondary vacuum. The shape of the A−D isotherms and the type of hysteresis loops were interpreted using the Brunauer et al.[7] model and de Boer[8] correlations, respectively, while specific surface areas were determined by the Brunauer−Emmett−Teller (BET)[9] method. The total pore volume of the mesoporous silica gels was calculated from desorption isotherm with the Barett−Joyner−Halenda (BJH) formula,[10] restricting the data field to relative pressure values close to unity ($0.35 < P/P_0 < 0.99$). The pore size distribution is thus given by the derivative of the desorbed volume as a function of the pore diameter.

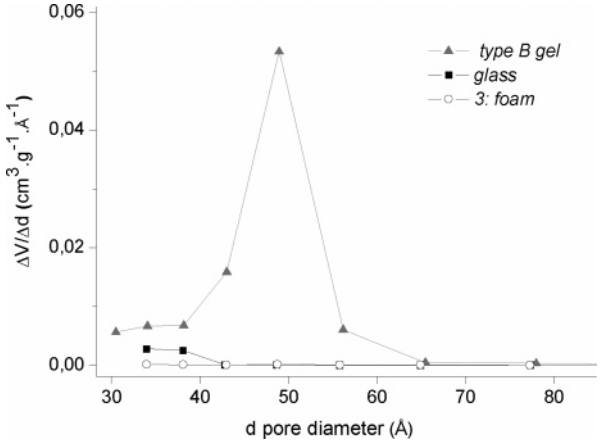

Figure 2. Pore-size distribution for: (△) stabilized xerogel at 850 °C (type A xerogel); (■) sol−gel-derived glass; (○) foamed silica xerogel (type C material).

II.2.4. IR Spectroscopic Investigations. The IR transmission spectra were recorded either through a thin slice of the silica sample (typical thickness: 50−70 μm) or through pellets of powdered silica diluted in KBr. To obtain a dry powder prior to the elaboration of the pellet, the silica monoliths were ground in acetone medium at room temperature and heated to 50 °C for 10 h to remove most of the organic pollution. The powder was then diluted at 25% in KBr and pressed into a pellet. The thin plates of silica were cut with a mechanical saw, polished, and finally rinced with acetone to remove most of the wax and oil. The spectra were recorded either on a Nicolet Avatar Fourier transform IR (FT-IR) spectrometer (pellets) or a Perkin-Elmer system 2000 FT-IR spectrometer (plates).

II.2.5. SEM and TEM Micrography. The microstructure of foamed samples was studied by SEM and TEM. SEM pictures were recorded using a Field Emission Gun SEM Hitachi S4700. To avoid the pollution induced by mechanical polishing, only cleaved surfaces were studied. A thin film of carbon was deposited on the surface before examination in order to eliminate the electrical charge. Samples were observed both with a chamber and in a lens secondary electron detector.

TEM observations were performed on a Philips CM 30 (300 kV). Thin foils used for TEM observations were prepared from slices by mechanical polishing to a thickness of 30 μm, followed by argon ion milling. A thin film of carbon was deposited on the foil before examination. Samples were also characterized using conventional microscopy and electron diffraction.

III. Results

III.1. Preliminary Note. The starting silica xerogels result from a 1-h stabilization treatment at 850 °C. The material is optically transparent, stable during several weeks, and exhibits a high porosity. The pore-size distribution for these xerogels is presented Figure 2. The mean BJH pore diameter reaches 50 Å with a BET surface averaging 400−600 m^2/g. The average density of the gels was evaluated to be 0.806 g/cm^3.

Two distinct structures have been identified during consolidation treatment of these xerogels depending on the procedures employed. A progressive heating (path 1 in Figure 1) yields a stable and clear glass after 11 h of isothermal heating at 1000 °C. The density of this final glass reaches 2.05 g/cm^3, and its Raman spectrum exhibits all the bands classically observed for the corresponding melt glass. However, if one heats the sample the "fast way", silica foam appears (path 2 in Figure 1) after only 5 h at 1000 °C.

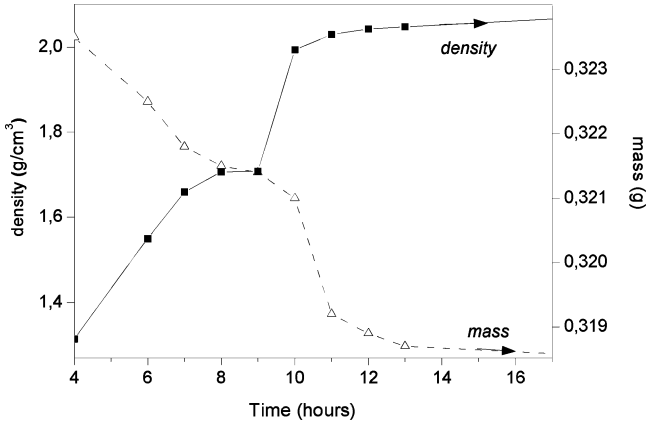

Figure 3. Weight loss and density values of the sol−gel-derived glass as a function of the heat-treatment time at 1000 °C. The temperature of 1000 °C was reached following the progressive heat-treatment.

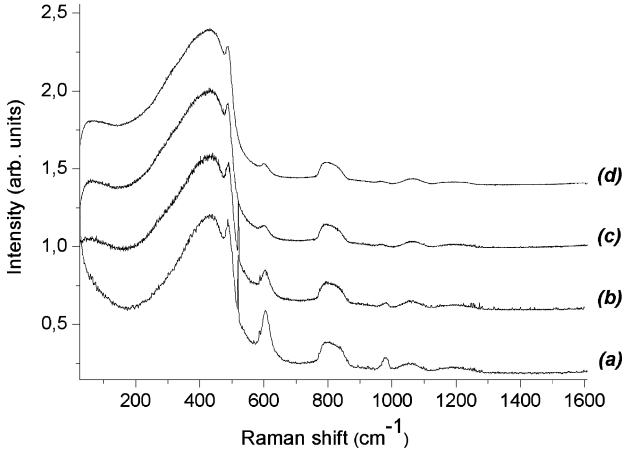

Figure 4. Raman spectra of silica xerogels after varying heat-treatment times at 1000 °C: (a) 4, (b) 7, (c) 10, and (d) 12 h. The temperature of 1000 °C was reached following the progressive heat-treatment.

III.2. Sol−Gel-Derived Glass.

III.2.1. Density Measurements. Although several routes yielding glass via the sol−gel process and their general mechanism have been reported,[11] it still remains quite complicated to obtain centimetric-sized uncracked monoliths. In this work, the sol−gel-derived glass was obtained by a "progressive" heating (Figure 1) with a better than 90% yield. The density of a silica gel is reported as a function of the time of heat-treatment at 1000 °C in Figure 3. The final density is reached after holding the sample at 1000 °C for 11 h. The curve exhibits a continuous increase in density from 1.3 g/cm^3 (4 h treatment) to the final value of 2.05 g/cm^3 after more than 12 h of annealing. This value is slightly lower than the typical density of melt-fused silica (2.2 g/cm^3). We attribute this difference to a probable residual porosity inside the final glass. The textural analysis (Figure 2) confirms this hypothesis: the final material contains a few mesopores (3−4 nm), which represent a mean total volume of 3×10^{-2} cm^3 per gram. The apparent weight of the sample decreases gradually between 4 and 9 h of treatment. This weight loss is attributed to the evaporation of water resulting from polycondensation reactions during densification. Between 8 and 10 h of heat treatment a steady state is observed. This plateau is accompanied by a dramatic increase of the apparent density (Figure 3), which corresponds to an important shrinkage with no significant mass loss. Such behavior has been mentioned by Hench and West,[11] but no experimental data have been provided. After 10 h of heat treatment, the volume reduction and the weight loss occur at the same rate, leading to a stabilized density of about 2.05. In section III.3, these variations will be discussed in correlation with the evolution of the gel structure at the nanometer scale. The final glass phase is quite stable since a further heat treatment (20 h at 1000 °C) does not influence either the sample appearance or its density (2.05 g/cm^3).

III.2.2. Raman Investigations. Detailed studies of the evolution of the Raman spectra of silica xerogels as a function of temperature have been reported for samples obtained using other synthesis procedures[12] based on the use of tetraethyl orthosilicate (TEOS) or TMOS under acidic conditions and with compositions different than the one reported in this paper. Figure 4 shows Raman spectra of a xerogel sample prepared in this work after isothermal heat-treatment of various lengths of time. The changes induced can be summarized as follows:

The intensities, of the sharp bands centered at 490 and 610 cm^{-1}, generally called "D_1 and D_2 defects bands", respectively, decrease continuously with heating time. These sharp bands are assigned to symmetric breathing modes of four- and three-membered silica rings,[13,14] respectively.

The band located at 980 cm^{-1} and associated with the Si−OH stretching mode drops in intensity with increasing heat-treatment time and almost vanishes after a treatment time of 12 h.

The main Raman band around 430 cm^{-1}, associated with a network Si−O−Si bending vibration, broadens gradually as a function of the heat-treatment time. This effect indicates an increase of the Si−O−Si angular distribution, attesting to a distortion of the silica network and a decrease of the local order.[13]

One can also observe the emergence of a low-frequency peak ($\sim$50 cm^{-1}) for xerogels heat treated for at least 7 h at 1000 °C (Figure 4). After this time, the intensity of this band evolves toward its final state, reached after 10 h of heat-treatment. This band, called the boson peak (BP), is characteristic of a vitreous structure. Several models[15,16] correlate the BP with the presence of nanometer-sized inhomogeneities within the glass matrix. In the model of Duval,[17] these entities consist of regions of cohesive structures in which vibrational excitations are localized. The position of the BP can be thus correlated with the average vibrational-mode frequency of the domains and hence to their average size. In the present study, the frequency of the BP remains identical for all heat-treatment times, suggesting the stability of the mean size of cohesive domains during densification.

The distinct increase in intensity of the BP between 9 and 10 h heating (see Figure 5) can be attributed either to an increase in the number of cohesive domains or to major changes arriving at the associated interfaces.[18] In any case, these effects attest to an appreciable distortion in the immediate environment of these domains. One might note that the steady state observed in the mass values (Figure 3) occurs at this same time. This combination of effects underlines the close connection existing between the shrinkage and the micro-organization of the silica network.

III.3. Silica Foam. Silica foam, a light and white solid, is the expanded form of the glass. The foam is characterized by its low density ($\rho \approx 0.3$ g/cm^3) and its highly macroporous structure. Type I foaming occurs during the densification of the gel, especially when the heating is very rapid, i.e., in a furnace preset to a high temperature. Figure 6 shows the different stages of foaming in a silica gel heat treated at 1000 °C for 5−15 h. Sample A corresponds to the xerogel described in section III.1 (density 0.806). The foaming phenomenon begins with an initial

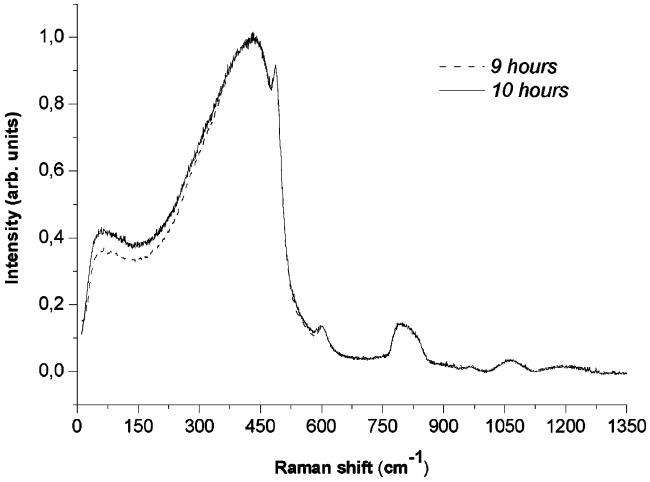

Figure 5. Raman spectra of silica samples after varying heat-treatment times at 1000 °C: (dashed line) 9 and (solid line) 10 h. The temperature of 1000 °C was reached following the progressive heat treatment.

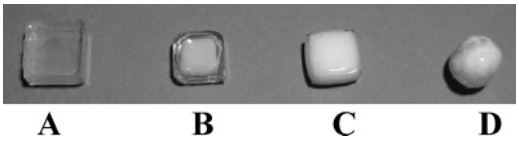

Figure 6. Appearance of sol−gel materials: (A) xerogel stabilized at 850 °C, (B) partially foamed material (heat-treatment time = 5 h at 1000 °C), (C) totally foamed material (heat-treatment time = 6 h at 1000 °C), and (D) expanded material (heat-treatment time = 15 h at 1000 °C). The temperature of 1000 °C was reached following the instantaneous heat treatment.

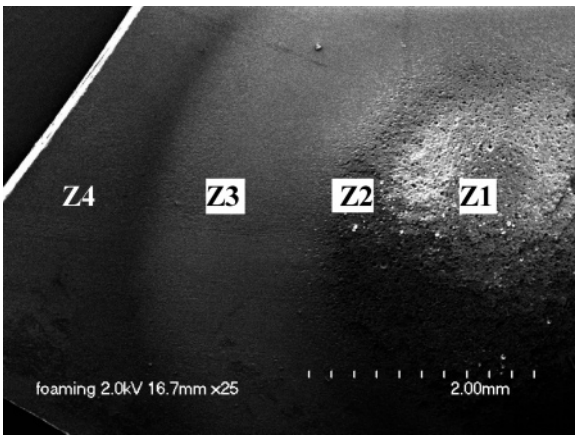

Figure 7. Scanning electron micrograph of the partially foamed xerogel (sample B). The area Z1 corresponds to the center of the sample, Z4 to the border, Z2 and Z3 to intermediate regions.

"white cloud" at the interior of the monolith, which gradually grows to fill the entire sample, leading finally to a bowl-like piece. Figure 7 shows the SEM micrograph of the partially foamed gel of Figure 6B. In the middle of the sample (area Z1 in Figure 7), the pore system, which is visible to the naked eye and is responsible for the opaque, white appearance of the monolith. From the SEM pictures the pore diameter distribution has been evaluated to be 2−100 μm. Points in area Z4 (the outer rim) represent a dense material with no pore system. Between these two zones, one can distinguish Z3, which corresponds to an intermediate state. The areas Z3 and Z1 are separated by a border zone we call Z2. This sequence of areas illustrates the diffusion−expansion phenomena of gas trapped inside the gel as advanced by Matsuyama et al.[5] to explain foaming in OH-containing glasses. A gas, which is shown in section III-3−3 to be water vapor, is trapped inside the matrix and expands the pores by pressurization when the annealing time is prolonged.

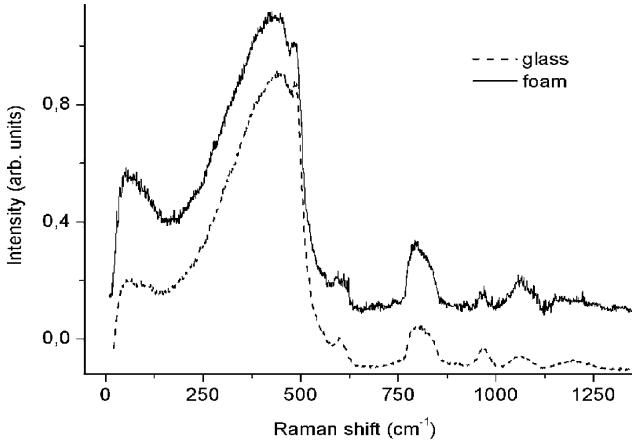

Figure 8. Raman spectra of (dashed line) a sol−gel derived glass obtained using a progressive heat treatment and (solid line) the totally foamed sample D.

The densities of a gel evolving toward bowl-like foam supplement these observations. Sample B, which results from 5 h of "fast" annealing, has a density gradient ranging from 1.5 g/cm^3 in the center to 2.05 at the edge. The next stage of foaming is illustrated by sample C, for which the density has been evaluated to 1.7 and which was obtained after 6 h of annealing. Finally, sample D, which represents the last and stable stage of the evolution (20 h at 1000 °C) has a final density of 0.3 g/cm^3. The densities of the zones Z1, Z2, Z3, and Z4 of the sample B were evaluated by using equivalent samples from which the zones were sliced and their densities measured. The densities of the samples A, C, and D were performed using the method described in the Experimental Section.

III.3.1. Textural Investigation. Nitrogen adsorption−desorption studies exhibit a very low physisorption of the adsorbent on the foam, leading to a flat isotherm and complete absence of open porosity (Figure 2). The BET specific surface was evaluated at 3.8 m^2/g. The foamed sample D is thus essentially made of dense glass that covers the macroporous structure, preventing any physisorption.

III.3.2. Raman Investigations. Raman spectra of a sol−gel-derived glass and a foamed sample obtained at 1000 °C are shown in Figure 8. Though the Raman spectrum of the totally foamed sample, the "expanded sample", designated by sample D (15 h of heat-treatment time) exhibits bands similar to those observed in the Raman spectrum of the sol−gel-derived glass, obtained via a the progressive heat-treatment procedure. However, one can still notice some variations between the two spectra: (1) The BP is more intense and narrower in the "expanded sample" spectrum, indicating that the interfaces of cohesive entities are more distorted and the domain size distribution of theses entities is narrower. (2) The bands D_1 and D_2 are weaker for the foamed sample, attesting to a decrease in the number of four- and three-membered silica. (3) The shape of the band located around 800 cm^{-1} is different for the two states. The intensity of the high-frequency region of this band (around 840 cm^{-1}) decreases in comparison with that of the low-frequency region (around 790 cm^{-1}) for the expanded sample. This behavior is related to a distortion of the Si−O−Si bridging angle (θ) leading to a structure in which the majority of the network Si−O−Si bonds are oriented at large θ values.[13] All these observations indicate that the expanded sample

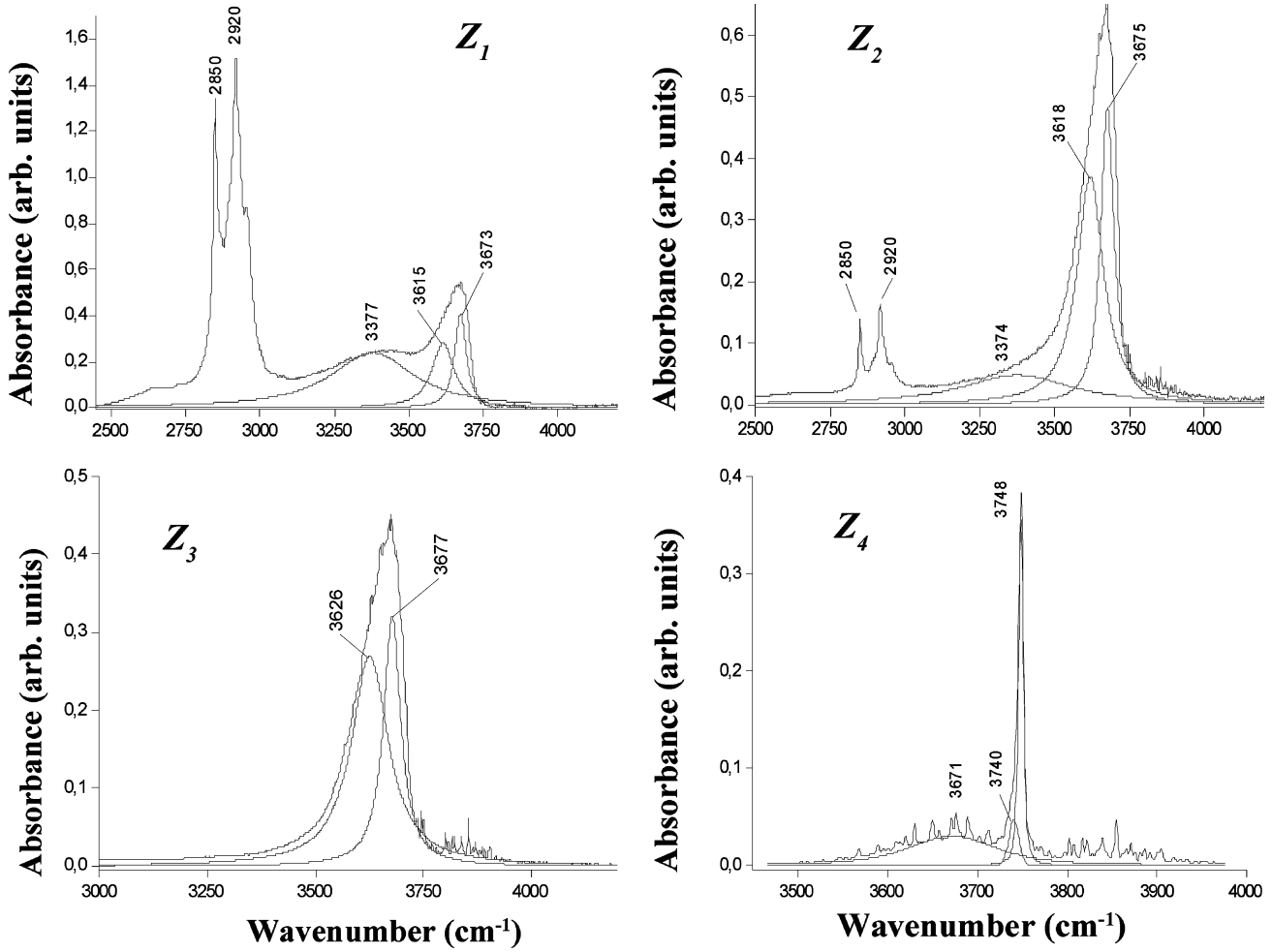

Figure 9. IR spectra of the zones shown in Figure 7 of the partially foamed sample B. The curve-fitted Gaussian peaks and the envelope formed by the summation of these peaks are also shown.

presents a globally amorphous structure, which is more strained than that of the sol−gel-derived glass.

III.3.3. IR Investigations. IR spectra were recorded of different areas of sample B (Figure 6), which exhibits both foamed and clear zones. These spectra were recorded using an infrared beam which diameter is equal to 1 mm in order to select different zones. Each IR spectrum (Figure 9) was curve fitted with Gaussian functions. The number of components for each band was chosen in order to take into account all the relevant OH-related species (free or bonded silanol groups, molecular water, etc.) existing in the foamed material.[19] The best fit was reached by minimizing the χ^2 parameter. In the present work, five components were used that can be assigned as follows: The wide band centered around 3370 cm^{-1} is attributed to the OH vibrational mode of molecular water.[19] The band centered around 3620 cm^{-1} can be attributed to OH vibrations of ≡Si−OH groups hydrogen-bonded with the ≡Si−O−Si≡ linkages and pairs of OH groups hydrogen-bonded with each other in linear configurations.[20] The component around 3675 cm^{-1} is due to Si−OH groups weakly bound to bridging oxygen atoms19. The two peaks at 3740 and 3748, observed only in the Z4 area, have been attributed by Takei et al.[21] to geminal hydroxyl groups and surface isolated (no H-bonding) silanols, respectively. In zones Z1 and Z2, two peaks, located at 2850 and 2920 cm^{-1} and attributed to C−H vibrations in alkyl groups are observed. Although organic components have been added to the mixture as solvent and drying control chemical additives, we exclude the assumption they might compose the foaming gas. Indeed, the IR spectrum of the xerogel is completely free of organic traces. Consequently, we impute these IR vibrations to pollution caused by the sample preparation.

One of the aims of the present paper is the determination of the concentrations of OH-related species. For this evaluation, intensities of bands at 3374, 3620, 3675, 3740, and 3748 cm^{-1} are used in the framework of a Beer−Lambert treatment

$$C = \frac{A}{\epsilon L} \tag{1}$$

where C [mol L^{-1}] is the concentration of a given species, A is the maximum of the corresponding absorbance band (unitless), ϵ is the extinction coefficient for that band [L mol^{-1} cm^{-1}], and L the path length through the sample material [cm]. Concentrations of hydroxyl groups that belong to weakly bonded silanols or molecular water were calculated from the absorbance of the bands at 3675 and 3374 cm^{-1}, respectively, in the IR spectra. The first band is generally used to determine the relative concentration of hydroxyl groups in vitreous silica. For calculations of the above-mentioned concentrations in ppm by weight, eq 1 can be written as follows

$$C_{\text{wtppm}} = 10^3 \frac{AM}{L\epsilon d} \tag{2}$$

where M is the molar mass of an OH group (17.01 g mol^{-1}), ϵ is the extinction coefficient at 3673 cm^{-1} (OH in silanols) or 3400 cm^{-1} (OH in water), and d is the density of the given zone in the silica sample. The extinction coefficients used in

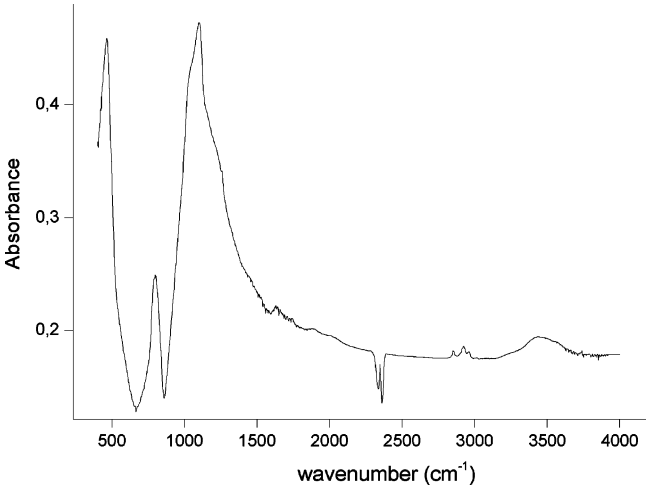

Figure 10. Typical IR spectrum of the totally foamed sample D (15-h heat treatment at 1000 °C).

the present paper were $\epsilon_{3670} = 77.5\ L_{glass}\ mol_{OH}^{-1}\ cm_{glass}^{-1}$ and $\epsilon_{3400} = 81\ L_{glass}\ mol_{OH}^{-1}\ cm_{glass}^{-1}$.[19]

Table 1 shows the resulting values for the concentrations of OH-related species in the four zones of sample B. The foamed area (Z1) exhibits high concentrations of both molecular water (3374 cm^{-1}) and hydroxyl groups (3670 cm^{-1}) inside the glass. With increasing distance from the center, the water content decreases drastically whereas the concentration of hydroxyl groups reaches a maximum at Z2 before decreasing gradually to about 300 ppm at the edge of the sample. Moreover, this latter part is the only zone where one can detect isolated surface silanols. Thus, the global evolution of all the OH-containing species follows a dramatic decay profile as a function of distance from the center, supporting the gas diffusion model.

These results indicate that the level of foaming is clearly linked to the amount of molecular water within the material. At the end of the foaming process (expanded material), only water contributes to the O−H vibrations as seen in the spectrum of Figure 10. By combination of the analyses of Figures 9 and 10, it appears that polycondensation of isolated silanols (3748 cm^{-1}) produces water that first enhances H bonded silanols (3675 cm^{-1}) and ends in the formation of molecular water and the loss of silanols.

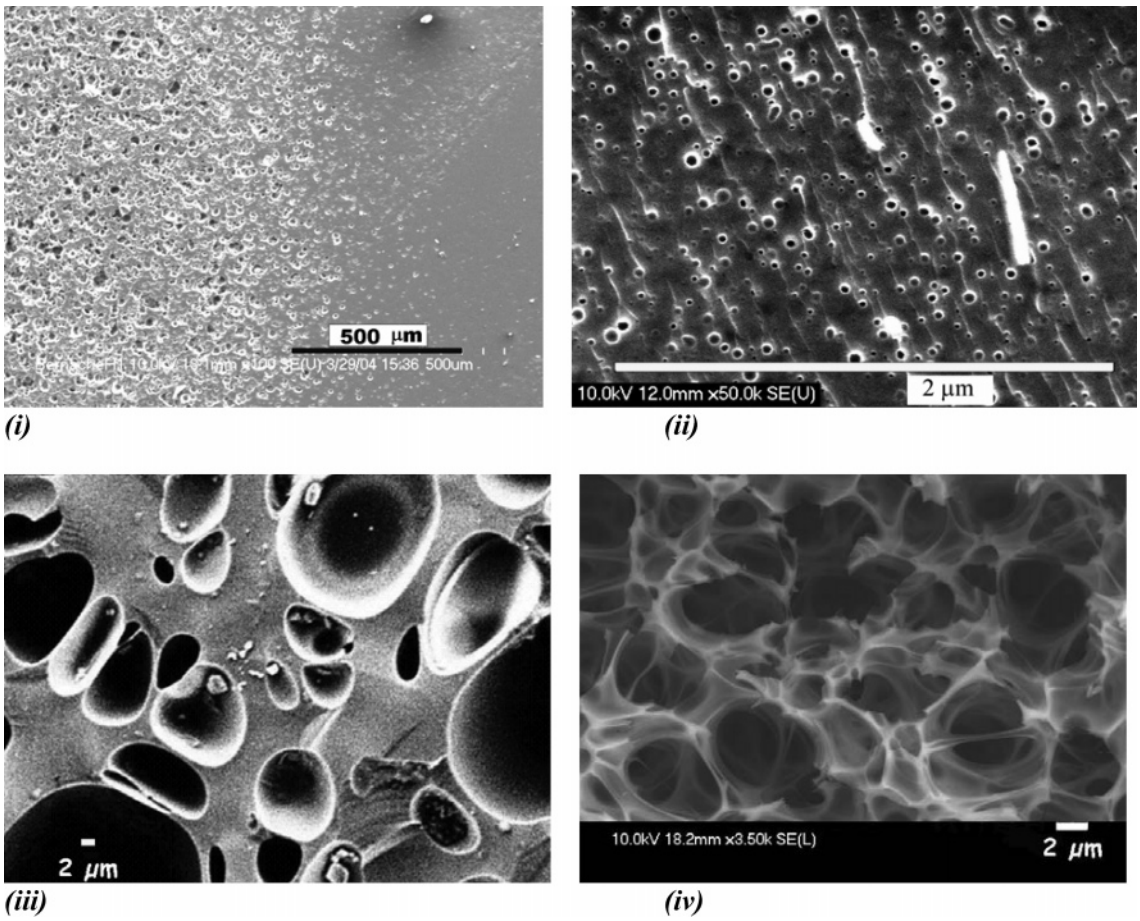

Figure 11. Scanning electron micrographs of (i and ii) the partially foamed sample B, (iii) the totally foamed sample C, and (iv) the expanded sample D.

TABLE 1: Estimation of the Concentrations of Water-Related Species as a Function of the Location in the Partially Foamed Silica Material B

	concentrations of water-related species (ppm)		
area in sample B	molecular water (3370 cm^{-1})	OH groups inside SiO_2 glass (3670 cm^{-1})	isolated surface OH groups (3748 cm^{-1})
Z1 (center, $d = 1.6$)	7500	8400	0
Z2 ($d = 1.75$)	1700	8600	0
Z3 ($d = 1.8$)	0	5600	0
Z4 (border, $d = 2$)	0	315	≠0*

III.3.4. Microstructural Observations.

III.3.4.a. SEM Observations. The SEM observations of Figure 11 were performed on the samples B, C, and D. All samples present similar microstructure composed of quasi-spherical porosity in the foamed region. For the partially foamed sample B, the number of the pores decreases gradually when moving away from the center (the center is at the left of Figure 11i). As molecular water is to be found at the interior of pores, the zone of the sample containing the most water must also be the zone of maximum porosity. Hence, the SEM observations are in good agreement with the spectroscopic data and support the previously proposed competition between water evacuation and densification.

When sintering begins, all remaining water is trapped inside the bulk of the material. The more centrally located, the more difficult its removal. At the first step of the foaming (sample B), the Figure 11ii shows that the porosity is composed of nanoscaled spherical bubbles (with an average diameter smaller than 10 nm) and by some micropores only detected at the center of the sample. In the case of sample C where the porosity has spread throughout, the SEM images of Figure 11iii show the expansion of the pores to a microscopic scale (average diameter 9 μm). At the end of the foaming process (sample D), the porous system is completely strectched and the sample has only a skeletal structure (see Figure 11iv). At this stage, the sample is entirely expanded and the density has reached its minimal value.

Detailed analysis of the intermediate stage of foaming reveals the presence of microscopic particles inside the pores (see Figure 11ii). By consideration of the preparation techniques, these particles cannot be due to pollution on the observed surface. However, the SEM analysis did not allow us to determine the organization of these inclusions, especially the possibility of the occurrence of a new phase during foaming.

III.3.4.b. TEM Observation. TEM studies of sample C (Figure 12) give the same indication of the structure as observed by SEM: spherical porosity separated by dense glass walls. Once again, in some cavities, grains are fixed at the surface. Quantitative observation was prevented by the nature of sample preparation: some particles may have been pulled out. Electron diffraction was performed to determine the crystallographic structure of the grains. Three different situations were observed:

(i) Figure 12a shows some aggregated sub-micrometric β-tridymite (P 6_3/m 2/m 2/c) grains enclosed in micrometric pores.

(ii) Isolated large micrometric α-cristobalite (P 4_1 2_1 2) crystals have been observed in some parts of the edge of the sample (See Figure 12b). It appears that this kind of grain is present in large pores (>10 μm).

(iii) The edge of some pores present nanocrystallites embedded in the glass matrix. The ring diffraction patterns performed on those nanocrystallites in such a region exhibit the β-tridymite structure (See Figure 12c).

The foamed material thus holds crystallites of different forms and sizes. The formation of these objects and their connections are not at this time obvious. One parameter that could contribute to this point is the water pressure inside the pores. This parameter can be roughly estimated, taking into account a starting amount of 4000 ppm OH in the silica sample and assuming spherical pores with a mean diameter equal to 4 nm. By use of the sample initial density of 1.9, it is thus easy to calculate the porous volume and the number of pores, which is approximatively 4×10^{18} cm^{-3}. Consideration that all of the silanol groups condense to yield water vapor inside the pores leads to a value of 1.5×10^{-23} moles of water, namely, about

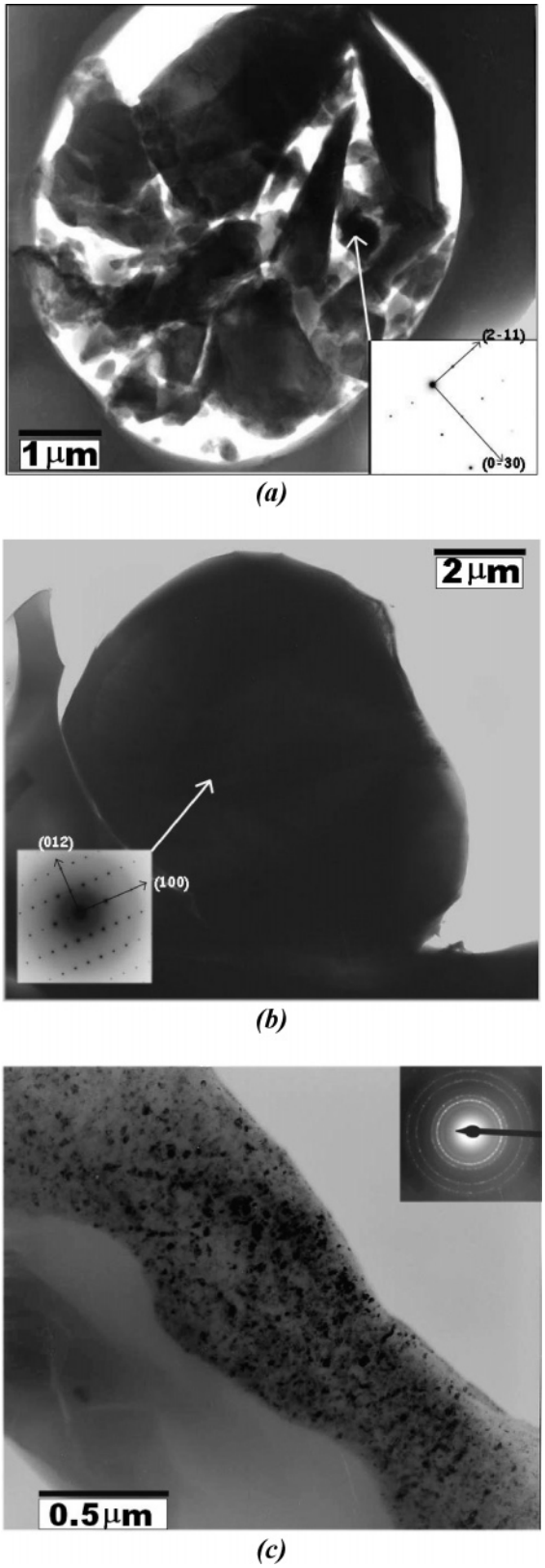

Figure 12. Transmission electron micrographs and electron diffraction patterns for different areas of the foamed sample C (a) inside micrometric pores, (b) at the edge of the sample, and (c) at the pore edge.

10 molecules per pore. The perfect gas equation can be then used to find the mean pressure of 4.8 Mpa. Such a pressure exceeding 10 atm makes possible a hydrothermal-like synthesis. Hence, The pore system behaves as a set of pressurized nanoreactors.

IV. Discussion

Previous observations[5,6] have already been cited of the foaming of silica xerogels. Type I foaming has been specifically presented to be related to three significant parameters: porosity, density, and OH content of the starting xerogels. Matsuyama et al.[5] argued that the foaming phenomenon does not occur for gels with a density lower than 1.0 g/cm^3, even if the concentration of OH groups is high enough. This conclusion was supported by the consideration that the pores in the low-density gels are quite large and thus the gas can easily escape from the sample. The foaming, based on the occurrence of gas trapped inside the matrix, is thus impeded. Kurumada et al.[6] observed a foamed structure only for materials synthesized under acidic conditions, attributing the absence of foaming in the "basic" gels to the large open porosity. By obtaining foams from a nondense, porous, and base-catalyzed xerogel, the present study allows us to reconsider the contribution of these parameters.

One of the most original results of the present study lies in the differences observed in the final state of xerogels synthesized under basic conditions, depending on whether the samples had been progressively or instantaneously heat treated at 1000 °C. Both of these heat treatments were carried out on similar xerogels and under the same sintering atmosphere. With starting materials exhibiting the same porosity, the same OH content and the same composition, the behavior was found to be determined only by the heat-treatment procedure. The progressive heat treatment converts xerogels into glasses, whereas instantaneous treatment results in a foamed structure. Moreover the foaming phenomenon can be split up into elementary steps, which have been observed successively by means of structural characterization, density measurements, the determination of OH-composition, and microstructural analysis.

When a given material is instantaneously heat treated at 1000 °C, the initiation of foaming takes place in the center of the sample and is viewed as a white cloud lying inside the monolith. The foaming is believed to be caused by trapped water vapor arising from the polycondensation of silanols located at the surface of the gel pores. The IR and Raman spectra confirm this statement, pointing out the presence of isolated silanols in the dense zone situated at the edges of the sample. These isolated OH groups would then be responsible for the remaining porosity inside the glass. In the middle of the sample, we have shown evidence of a high concentration of water but no residual isolated silanols. Hence, the degree of foaming is greater in the areas where the water concentration is higher. We attribute the variation in the degree of foaming to the difference of time required for the densification process, compared to that necessary for the diffusion of the water vapor before the pore closure. Thus the water vapor generated near the surface of the sample escapes easily before the pores collapse, leading to a dense glassy structure. In this case, the diffusion rate of water leaving the sample is greater than the rate of densification. As far as the gas formed in the center of the gel is concerned, we assume that the densification process is faster than the vapor diffusion. Polycondensation still occurs, leading to an increase in water content and consequently to the pressurization of the vapor trapped inside the pores. These pores then undergo expansion and aggregation processes as the heat-treatment time at 1000 °C increases. The final stage of silica foam has been found to be non dense (0.3 g/cm^3).

The structural stability of the foamed materials at the nanometer scale had not been previously discussed in the literature, insofar as authors considered the foam to contain no OH groups and to be nonporous and vitreous by nature. In the present work, though the Raman investigations indicate that the foamed materials have a globally amorphous structure, the TEM microscopy reveals the presence of crystallites that are prone to nucleation and growth processes. These crystallites present both β-tridymite and α-cristobalite structures. This statement is in good agreement with the classical evolution of powdered silica phases that can be resumed as follows: for temperatures below 1000 °C, the silica is amorphous and above 1400 °C, the material is fully crystallized in the β-cristobalite phase. The intermediate stage consists of a series of mixtures, containing successively glass, α- and β-tridymite and α-cristobalite. The observed shift of the glass-to-cristobalite phase-transition temperature in the case of monolithic samples may be attributed to the high water pressure found in the pores of the material, compensating for the considerable lower thermal energy involved.

V. Conclusion

In this contribution, we have proved that a combination of several parameters has to be considered in order to predict the evolution of silica xerogels. Even though the starting xerogels may be perfectly similar (same porosity, same OH-content, same composition), we have observed that applying slightly different heating procedures (based on the change of the heating rate) under the same atmosphere could yield totally different materials. In concern with the study of the foaming phenomenon in silica xerogels, we suggest that the heating rate should be included as an essential parameter in addition to porosity, OH content, and density in the controls the sintering kinetics.

The OH contents have been evaluated by IR spectroscopy in samples at different stages of foaming and the results are found to support the heat-related water diffusion in silica. Thus the diffusion of water in the structure has to be taken into account together along with the size of the monolith. We have demonstrated also that foamed silica materials are unstable when a heat treatment is pursued at high temperatures. The structure of such matrixes has been found to evolve from an amorphous state to a partially crystallized one.

Acknowledgment. The Centre d'Etudes et de Recherches Lasers et Applications is supported by the Ministère Chargé de la Recherche, the Région Nord/Pas de Calais. and the Fonds Européens de Développement Economique des Régions (FEDER). The microscopes have been supported by the FEDER program. The present study is supported by the Région Nord/Pas de Calais. The authors thank Dr. Gauvin for his help with the infrared investigations and his fruitful discussions.

References and Notes

(1) Armellini, C.; Ferrari, M.; Montagna, M.; Pucker, G.; Bernard, C.; Monteil, A. *J. Non-Cryst. Solids* **1999**, *245*, 115.

(2) Ferrer, M. L.; Yuste, L.; Rojo, F.; del Monte, F. *Chem. Mater.* **2003**, *15* (19), 3614.

(3) Sherer, G. W.; Brinker, C. J. *Sol−Gel Science: The Physics and Chemistry of Sol−Gel Processing*; Academic Press: New York, 1990; Chapter 11, p 675.

(4) Mackenzie, J. D. *J. Non-Cryst. Solids* **1982**, *48*, 1.

(5) Matsuyama, I.; Susa, K.; Satoh, S.; Goo, J. K. *J. Non-Cryst. Solids* **1992**, *151*, 160.

(6) Kurumada, K. I.; Kitao, N.; Tanigaki, M.; Susa, K.; Hiro, M. *Langmuir* **2004**, *20*, 4771.

(7) Brunauer, S.; Deming, L. S.; Deming, W. S.; Teller, E. *J. Am. Chem. Soc.* **1940**, *62* (7), 1723.

(8) De Boer, J. H. *The Structure and Properties of Porous Materials*; Butterworths: London, 1958; p 68.

(9) Brunauer, S.; Emmett, P. H.; Teller, E. *J. Am. Chem. Soc.* **1938**, *60*, 309.

(10) Barret, E. P.; Joyner, L.; Halenda, P. P. *J. Am. Chem. Soc*. **1951**, *73* (1), 373.
(11) Hench, L. L.; West, J. K. *Chem. Rev*. **1990**, *90*, 33.
(12) Colomban, Ph. *J. Raman Spectrosc.* **1996**, *27*, 747.
(13) Nedelec, J.-M; Bouazaoui, M.; Turrell, S. *J. Non-Cryst Solids* **1999**, *243*, 209.
(14) Kinowski, C.; Bouazaoui, M.; Bechara, R.; Hench, L. L.; Nedelec J.-M.; Turrell, S. *J. Non-Cryst. Solids* **2001**, *291*, 143.
(15) Duval, E.; Mermet, A; Surovtsev, N. V.; Dianoux, A. J. *J. Non-Cryst Solids* **1998**, *235*−*237*, 203.
(16) Benassi, P.; Fontana, A.; Frizzera, W.; Montagna, M.; Mazzacurati V.; Sognorelli G. *Philo. Magn.* **1995**, *B71*, 761.
(17) Duval, E.; Boukenter, A.; Achibat, T. *J. Phys. Condens. Matter* **1990**, *2*, 10227.
(18) Mermet, A. Ph.D. Thesis, Université Lyon, 1996.
(19) Davis, K. M.; Tomozawa, M. *J. Non-Cryst. Solids* **1996**, *201*, 177.
(20) Poltnichenko, V. G.; Sokolov, V. O.; Dianov, E. M. *J. Non-Cryst. Solids*, **2000**, *261*, 186.
(21) Takei, T.; Kato, K.; Meguro, A.; Chikazawa, M. *Colloids and Surfaces* **1999**, *150*, 77.